ELSEVIER

Inorganica Chimica Acta 243 (1996) 19–24

Inorganica Chimica Acta

Kinetics, mechanism and thermodynamics of iron carbon bond dissociation in organoiron porphyrin complexes[1]

Charles G. Riordan[2], Jack Halpern*

Department of Chemistry, University of Chicago, Chicago, IL 60637, USA

Abstract

Thermolysis of Fe(P)R (P = octaethylporphyrinato dianion, R = C_6H_5, CH_3, C_2H_5, $CH_2C(CH_3)_3$; P = tetraphenylporphyrinato dianion, R = C_6H_5; P = tetra(*p*-tolyl)porphyrinato dianion, R = C_6H_5) in benzene yielded Fe(P) and RH quantitatively. Rate-limiting homolytic iron–carbon bond dissociation kinetics were determined by competitive trapping of the carbon radicals with Ph_3SnH: $Fe(P)R + Ph_3SnH \xrightarrow{\Delta} Fe(P) + RH + 1/2Ph_6Sn_2$. Determination of the temperature dependence of the limiting rates of the trapping reactions yielded the following bond dissociation activation enthalpies $\Delta H^{\ddagger}_D$(Fe–R): R = C_6H_5, 33 kcal mol^{-1}, CH_3, 23 kcal mol^{-1}, C_2H_5, 19 kcal mol^{-1}, $CH_2C(CH_3)_3$, 17 kcal mol^{-1}. Assuming diffusion-limited Fe(P), R$^{\cdot}$ recombination, the corresponding Fe(P)–R bond dissociation energies were estimated to be ca. 2 kcal mol^{-1} lower than these values. Addition of the axial ligands, L, yielded six-coordinate species, $LFe(P)CH_3$ (L = py, PEt_3) and accelerated the rate of iron–carbon bond homolysis.

Keywords: Iron complexes; Porphyrin complexes; Kinetic measurements

1. Introduction

Organoiron compounds containing iron–carbon σ-bonds have been invoked in several biological systems, notably as intermediates in lipoxygenase oxidations [1] and heme inactivation in hemoglobin, myoglobin, cytochrome P450 and catalase by the suicide inhibitor, phenylhydrazine [2]. It has been suggested that the inactivation mechanism involves formation of a σ-bonded iron-phenyl complex followed by oxidative migration of C_6H_5 from iron to the nitrogen of the porphyrin as the protein denatures. Model studies using synthetically accessible porphyrins have helped define likely intermediates of the phenylhydrazine oxidation which ultimately produces the organometallic complex [2]. Mansuy [3] has characterized the bis(phenylhydrazine) derivative, Fe(TPP)-$(C_6H_5NHNH_2)_2$ (TPP = tetraphenylporphyrinato dianion) and selectively oxidized it to first, the bis(phenyldiazene), $Fe(TPP)(C_6H_5NNH)_2$, and then to $Fe(TPP)C_6H_5$. The oxidative migration of the C_6H_5 group, which ultimately is responsible for protein denaturing, also has been well defined in model studies [2]. $Fe(P)C_6H_5$ (P = TPP, OEP = octaethylporphyrinato dianion) undergoes a one electron oxidation to $Fe(P)C_6H_5^+$, followed by phenyl migration to nitrogen analogous to the metal-to-ligand migration that has previously been demonstrated to follow oxidation of alkylbis(dimethylglyoximato)cobalt complexes [4]. A second one electron oxidation yields stable $Fe^{III}(P\text{–}NC_6H_5)^{2+}$. Reduction of the N-phenylated complex facilitates back-migration to regenerate Fe(P)-C_6H_5.

Alkyliron porphyrin complexes, Fe(P)R, may be synthesized by several routes [5]. They undergo Fe–R insertion reactions with a variety of small molecules including O_2, CO_2, CO and SO_2 [6]. The trend of CO insertion rates, alkyl > CH_3 >>> C_6H_5, parallels the typical trend of decreasing metal-carbon (e.g. Co–R) bond dissociation energies consistent with a pathway triggered by Fe–R bond homolysis analogous to that for the insertion of O_2 into Co–R bonds [7]. While other recent studies provide fairly convincing qualitative evidence for reversible iron–alkyl bond homolysis [8], there clearly is a need for

* Corresponding author.

[1] Dedicated to Professor Harry Gray on the occasion of his sixtieth birthday.

[2] Current address: Department of Chemistry, Kansas State University, Manhattan, KS 66506, USA.

0020-1693/96/$15.00
SSDI 0020-1693(95)04887-4

quantitative information about the kinetics and energetics of such dissociation reactions.

The present study is designed to address this need by determining the iron–carbon bond dissociation rates and energies of a range of (L)Fe(P)R complexes in which the alkyl or aryl ligand (R), the axial base (L), and the porphyrin ring (P) were varied systematically. We have employed the kinetic method previously used extensively to determine cobalt–carbon bond dissociation energies [9,10]. This involves determination of the kinetics of homolytic dissociation of the iron–carbon bond upon thermolysis of Fe(P)R, using a suitable trap, in this case Ph_3SnH, to capture the alkyl radical in competition with recombination with Fe(P) (Eqs. (1) and (2)). Confirmation of this scheme was provided by the kinetic behavior and product characterization.

$$\mathrm{Fe(P)R} \underset{k_{-1}}{\overset{k_1}{\rightleftharpoons}} \mathrm{Fe(P)} + \mathrm{R}^{\bullet} \qquad (1)$$

$$\mathrm{R}^{\bullet} + \mathrm{Ph_3SnH} \xrightarrow{k_2} \mathrm{RH} + \mathrm{Ph_3Sn}^{\bullet} \qquad (2)$$

$$\mathrm{Ph_3Sn}^{\bullet} \xrightarrow{\text{fast}} 1/2\mathrm{Ph_6Sn_2} \qquad (3)$$

2. Results

The general pattern of thermolysis of this class of compounds is exemplified by that of $Fe(OEP)CH_3$. Thermolysis of $Fe(OEP)CH_3$ in benzene or toluene yielded Fe(OEP) and CH_4 quantitatively as determined by UV-visible and ^1H NMR spectroscopies. In the presence of Ph_3SnH as a free radical trap, the products of thermolysis of $Fe(OEP)CH_3$ were Fe(OEP), CH_4 and Ph_6Sn_2 (determined by ^{119}Sn NMR) in accord with Eq. (4).

$$\mathrm{Fe(OEP)CH_3} + \mathrm{Ph_3SnH} \xrightarrow{\Delta} \mathrm{Fe(OEP)} + \mathrm{CH_4} + 1/2\mathrm{Ph_6Sn_2} \qquad (4)$$

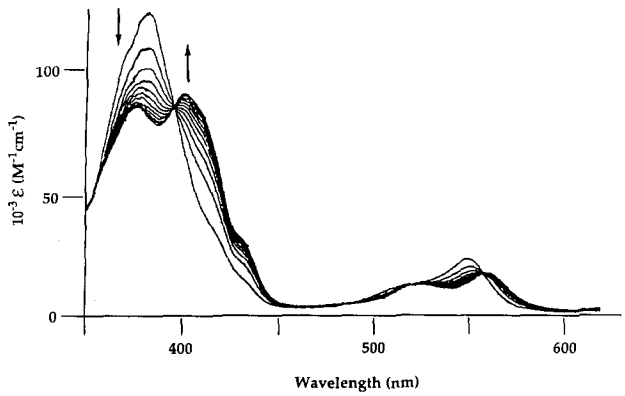

Fig. 1. Electronic spectral changes accompanying the thermolysis of $Fe(OEP)CH_3$ (5.0×10^{-5} M) in the presence of Ph_3SnH (1.0×10^{-3} M) in benzene at 50°C. Spectra were recorded at 60 s intervals.

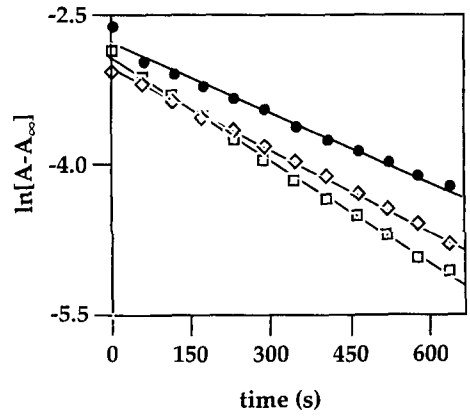

Fig. 2. First order plots of disappearance of $Fe(OEP)CH_3$ (5.0×10^{-5} M initially) in benzene at 70°C in the presence of Ph_3SnH: (●) = 2.0×10^{-2} M, (◇) = 2.0×10^{-3} M, (□) = 4.0×10^{-4} M.

The spectroscopic changes accompanying the reaction are depicted in Fig. 1. The decomposition of $Fe(OEP)CH_3$, monitored by UV-visible spectroscopy at 550 nm, exhibited first order kinetics over at least three half-lives (Fig. 2). The rate of decomposition increased with increasing [Ph_3SnH] to a limiting value (typically at >0.02 M Ph_3SnH) (Fig. 3). Similar trapping of the CH_3 radical was observed using 2,2,6,6-tetramethylpiperdine-*N*-oxide (TEMPO) as free radical trap. The products of this first order reaction were CH_3–TEMPO and $[Fe(OEP)]_2O$, the latter formed in a secondary reaction between Fe(OEP) and TEMPO. At 50°C, the limiting rate constant for trapping by TEMPO, $k_{obs} = 5.9 \times 10^{-4}$ s^{-1}, agreed well with that for trapping by Ph_3SnH, $k_{obs} = 6.2 \times 10^{-4}$ s^{-1}. These results can be accommodated by the mechanism of Eqs. (1)–(3), according to which the rate of decomposition of $Fe(OEP)CH_3$ is given by

$$\frac{-\mathrm{d[Fe(OEP)CH_3]}}{\mathrm{d}t} = k_{obs}[\mathrm{Fe(OEP)CH_3}] = \frac{k_1 k_2 [\mathrm{Fe(OEP)CH_3}][\mathrm{Ph_3SnH}]}{k_1[\mathrm{Fe(OEP)}] + k_2[\mathrm{Ph_3SnH}]} \qquad (5)$$

with

$$k_{obs} = \frac{k_1 k_2 [\mathrm{Ph_3SnH}]}{k_1[\mathrm{Fe(OEP)}] + k_2[\mathrm{Ph_3SnH}]} \qquad (6)$$

In the limiting regime when $k_2[Ph_3SnH] >> k_{-1}[Fe(OEP)]$, $k_{obs} \approx k_1$. Consistent with the above mechanism, addition of independently prepared Fe(OEP) resulted in a slowing of the decomposition reaction. With added Fe(OEP) and Ph_3SnH under pseudo-first order conditions, i.e. [Fe(OEP)], [Ph_3SnH] >> [$Fe(OEP)CH_3$], the decomposition kinetics were consistent with competitive trapping of $CH_3^{\bullet}$ by Fe(OEP) and Ph_3SnH as exemplified by the linear plots of $1/k_{obs}$ versus [Fe(OEP)]/[Ph_3SnH] (Eq. (7), Fig. 4).

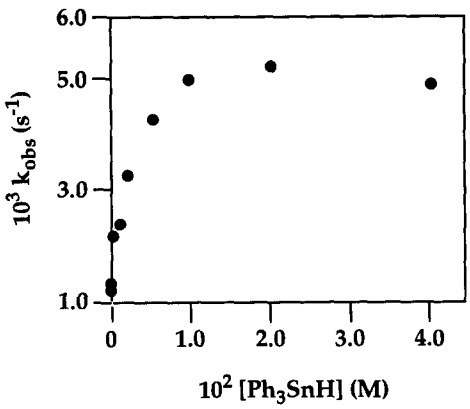

Fig. 3. Plot of k_{obs} versus [Ph_3SnH] for the thermolysis of Fe(OEP)CH_3 in benzene at 70°C. Initial [Fe(OEP)CH_3] = 1.0×10^{-5} to 5.0×10^{-5} M; [Ph_3SnH] = 0, 0, 0.4, 1.0, 2.0, 2.0, 5.0, 10, 20, 40 mM.

$$\frac{1}{k_{obs}} = \frac{1}{k_1} + \frac{k_{-2}}{k_1 k_2}\left(\frac{[Fe(OEP)]}{[Ph_3SnH]}\right) \quad (7)$$

When combined with independently determined values of k_2 from measurements of rates of trapping of free radicals by Ph_3SnH [11], these results yielded values for the recombination rates, k_{-1}, listed in Table 1. These are in the same range as rate constants for other metal alkyl radical recombinations [10] and consistent with the value of 3.9×10^9 M^{-1} s^{-1} reported by Brault and Nexa for the combination of $CH_3^{\bullet}$ with Fe(deuteroporphyrin) [12].

The activation parameters, $\Delta H^{\ddagger}$ and $\Delta S^{\ddagger}$, were determined from rate measurements under the limiting condition, $k_{obs} \approx k_1$, no added Fe(OEP), over the temperature range 50–75°C. The results are summarized in Table 2.

Since values of k_{-1}, where measured, are in the diffusion-controlled regime, $\Delta H^{\ddagger}_{-1}$ may be approximated by $\Delta H^{\ddagger}$ of viscous flow which, for solvents such as benzene, is ca. 1–2 kcal mol^{-1}. Applying this correction yields the bond dissociation energies listed in Table 1. These range from 15 to 31 kcal mol^{-1}.

2.1. Thermolysis in the presence of added base

2.1.1. Pyridine

Addition of pyridine-d_5 to Fe(OEP)C_2H_5 at 22°C resulted in immediate and quantitative formation of Fe(OEP)py_2 and C_2H_4 as determined by ^1H NMR. Similar addition of pyridine-d_5 to the CH_3 and C_6H_5 derivatives however, yielded six-coordinate species, i.e. (py)Fe(OEP)R. Addition of pyridine to benzene solutions of Fe(OEP)CH_3 resulted in UV-visible spectroscopic changes consistent with those reported for Fe(OEP)C_6H_5 [13]. Thermolysis of Fe(OEP)CH_3 in the presence of pyridine, with Ph_3SnH as added trap conformed to the stoichiometry of Eq. (8) and exhibited first order kinetics. At 70°C, with [Ph_3SnH] > 2×10^{-2} M, the rate of decomposition increased with increasing [pyridine] to a limiting rate constant of 1.5×10^{-2} s^{-1} at >2.0 M pyridine. Assuming a rapid equilibrium between Fe(OEP)CH_3 and (py)Fe(OEP)CH_3, the relation between k_{obs}, the individual rate constants, k_1 and k_{py}, and the dissociation constant, K_D, is given by Eq. (9).

(py)Fe(OEP)CH_3 + Ph_3SnH →

$$Fe(OEP)py_2 + CH_4 + 1/2Ph_6Sn_2 \quad (8)$$

$$\frac{1}{k_{obs} - k_1} = \frac{1}{k_{py} - k_1} + \frac{K_D}{k_{py} - k_1[pyridine]} \quad (9)$$

The plot of k_{obs} versus [pyridine] in Fig. 5 exhibits the predicted saturation kinetics behavior, with the best fit to Eq. (9) obtained using the values $k_{py} = 1.56 \times 10^{-2}$ s^{-1} and $K_D = 0.44$ M^{-1}. Measurement of k_{obs} in the limiting regime, [pyridine] > 2.0 M, at temperatures ranging from 50 to 70 °C yielded $\Delta H^{\ddagger} = 21.9$ kcal mol^{-1} and $\Delta S^{\ddagger} = -3.2$ cal $mol^{-1}°K^{-1}$ (Tables 3 and 4).

2.1.2. PEt_3

Addition of PEt_3 to benzene solutions of Fe(OEP)CH_3 resulted in a color change from rose to orange and formation of (PEt_3)Fe(OEP)CH_3 as determined by UV-visible and ^1H NMR spectroscopies. Thermolysis in the presence of Ph_3SnH yielded Fe(OEP)$(PEt_3)_2$, CH_4 and Ph_6Sn_2. Well behaved first order kinetics were observed. A plot of k_{obs} versus [PEt_3] at 20°C exhibited saturation kinetics at [PEt_3] > 0.2 M (Fig. 6). The data are best accommodated with $k_{PEt_3} = 9.7 \times 10^{-3}$ s^{-1} and $K_D = 1.6 \times 10^{-3}$ M^{-1}. Activation parameters, determined from measurements of

Table 1

Rate constants, activation parameters and bond dissociation energies for Fe(OEP)R complexes

R	k_1 (s^{-1}, 25°C)	k_{-1}/k_2 (T,°C)[a]	k_{-1} (M^{-1} s^{-1})	$\Delta H^{\ddagger}$ (kcal mol^{-1})	$\Delta S^{\ddagger}$ (cal (mol K)$^{-1}$)	D_{Fe-R} (kcal mol^{-1})
CH_3	2.5×10^{-5}	155 (70)	1.4×10^9	23.3 ± 0.4	−1.1 ± 1.2	21
C_2H_5	1.0×10^{-3}	117 (60)	1.0×10^9	18.6 ± 0.6	−9.3 ± 1.7	17
$CH_2C(CH_3)_3$	3.8×10^{-2}	998 (15)		17.3 ± 1.4	−6.6 ± 4.8	15
C_6H_5	3.8×10^{-11}			33.0 ± 1.2	4.5 ± 2.9	31

[a]Temperature at which the ratio k_{-1}/k_2 was measured.

Table 2
Temperature dependence of k_{obs} for thermolysis of Fe(OEP)R in the presence of limiting concentration of Ph_3SnH

R	T (°C)	$10^3 k_1$ (s^{-1})
CH_3	50	0.62
	55	1.0
	60	1.8
	60	1.8
	65	3.3
	70	5.1
	70	5.2
	70	5.4
	75	8.7
C_2H_5	40	0.50
	45	0.86
	50	1.2
	50	1.3
	55	2.1
	60	3.4
	65	4.9
$(CH_3)_3CCH_2$	10	7.2
	15	13
	15	13
	20	21
	20	23
	25	48
	25	50
	30	52
	30	57
C_6H_5	118.5	0.03
	118.5	0.04
	137	0.24
	141	0.31
	141	0.35
	145	0.52
	150	0.81

limiting rates over the range 5 to 25°C, are contained in Table 4.

Kinetic measurements in the presence of added ligand to $Fe(OEP)CH_3$ provide a convenient method for determining the decomposition rate constants of in situ prepared 6-coordinate complexes which are difficult to isolate due to low binding affinities for the axial ligands.

3. Discussion

3.1. Factors influencing bond dissociation energies

3.1.1. Alkyl or aryl ligand

The trend of decreasing bond dissociation energies of the alkyl derivatives in going from CH_3 (21 kcal mol^{-1}) to C_2H_5 (17 kcal mol^{-1}) to $CH_2C(CH_3)_3$ (15 kcal mol^{-1}) is readily rationalized by the steric requirements of the alkyl groups and is in good agreement with corresponding Co–R values [10]. The Fe(P)–R bond dissociation energies determined here are significantly weaker (ca. 10–15 kcal mol^{-1}) than the Co derivatives. The stronger iron–aryl bond compared with the corresponding iron–alkyl bond, is consistent with several other reported such comparisons [14].

The overriding importance of steric factors in influencing Fe–R bond dissociation energies in this system is best exemplified by comparing $Fe(OEP)C_6H_5$ to $Fe(OEP)o\text{-}C_6H_4CH_3$. Limiting thermolysis rates at 90°C are 2.0×10^{-7} s^{-1} for C_6H_5 and 3.0×10^{-4} s^{-1} for $o\text{-}C_6H_4CH_3$. Assuming similar entropic contributions, the 1000-fold increase in rate observed roughly corresponds to a 3–5 kcal mol^{-1} weaker Fe–$o\text{-}C_6H_4CH_3$ bond. Parallel differences of ca. 8 kcal mol^{-1} have previously been reported between corresponding Co–$CH_2C_6H_5$ and Co–$CH(CH_3)C_6H_5$ bond dissociation energies [15].

3.1.2. Axial ligand

Table 4 summarizes the differences in the limiting thermolysis rate constants for $Fe(OEP)CH_3$ (in the absence of added axial ligand) and $LFe(OEP)CH_3$ where L = pyridine or PEt_3. The range of observed bond dissociation energies is small corresponding to a difference of 3 kcal mol^{-1} between $Fe(OEP)CH_3$ and its PEt_3 derivative. At 25°C, these correspond to a difference of limiting thermolysis rates of ca. 1.7×10^4. Base ligation to $Fe(OEP)CH_3$ could result in substantial displacement of the metal center relative to the porphyrin plane to accommodate the sixth ligand. In $Fe(TPP)C_6H_5$, the only structurally characterized organoiron porpyrin derivative to date, the iron is 0.17 Å out of the porphyrin plane [16]. Upon ligand binding, the metal is expected to be pulled towards the *trans*-axial ligand. This could influence the Fe–CH_3 bond length and bond dissociation energy due to the increased repulsion between the methyl group and the porphyrin. Somewhat different patterns of axial ligand (L) dependence have been determined for $C_6H_5CH_2$-

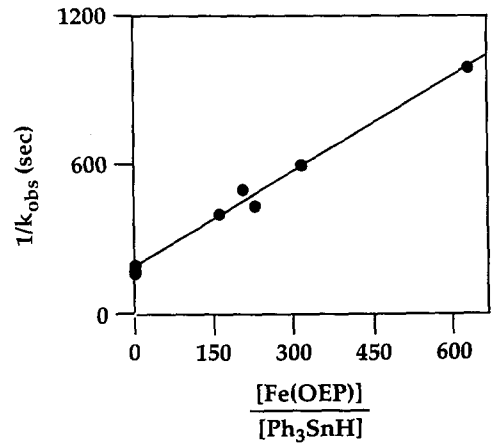

Fig. 4. Plot of $1/k_{obs}$ versus [Fe(OEP)]/[Ph_3SnH] for the thermolysis of $Fe(OEP)CH_3$ at 70°C in the presence of added Fe(OEP). Concentrations were [$Fe(OEP)CH_3$] = 1.0×10^{-6} M for all reactions; [Fe(OEP)] = 0, 0, 0, 1.4×10^{-5}, 1.0×10^{-5}, 2.8×10^{-5}, 2.8×10^{-5}, 2.8×10^{-5} M and [Ph_3SnH] = 0.01, 0.02, 0.04, 0.002, 0.001, 0.003, 0.002, 0.001 M, respectively.

Table 3

Temperature dependence of k_{obs} for thermolysis of $Fe(OEP)CH_3$ in the presence of limiting concentration of added ligand

Ligand	T (°C)	10^2k (s^{-1})
py	50	0.20
py	60	0.50
py	65	1.04
py	70	1.48
PEt_3	5	0.13
PEt_3	10	0.28
PEt_3	20	1.00
PEt_3	20	1.04
PEt_3	25	1.57

$Co(DH)_2L$ (DH_2 = dimethylglyoxime), $C_6H_5CH(CH_3)$–$Co(DH)_2L$ and $C_6H_5CH_2$–Co(OEP)L [17]. Thus for $C_6H_5CH_2$–Co(OEP)L, $k_{25°} = 2 \times 10^{-11}$ s^{-1} (no axial ligand), 6×10^{-9} (L = PBu_3) and 6.5×10^{-7} (L = pyridine).

3.1.3. Porphyrin

At 125°C in mesitylene, the limiting thermolysis rate constants for the series Fe(P)Ph are 6.2×10^{-5} s^{-1} (OEP), 4.2×10^{-4} s^{-1} (TTP) and 1.4×10^{-3} s^{-1} (TPP). While the range of these values is small, the trend, TPP > TTP > OEP, is in qualitative agreement with the corresponding Fe^{III}/Fe^{II} redox potentials [18] or porphyrin basicities; the Fe(P)–C_6H_5 bond dissociation energy increasing with ligand basicity. The trend parallels that obtained for cobalt complexes [15b].

4. Experimental section

Elemental analyses were performed by Galbraith Laboratories Inc., Knoxville, TN. Benzene, toluene and THF were distilled from Na benzophenone ketyl. Mesitylene and pyridine were distilled from Na. Ph_3SnH and Me_4Sn were purchased from Aldrich Chemical Co. and used without further purification. Grignard reagents were used as received from Aldrich Chemical Co. or prepared from RBr and Mg in THF. Fe(P)R (P = octaethylporphyrinato, tetraphenylporphyrinato and tetra-*p*-tolylporphyrinato) were synthesized from Fe(P)Cl and the appropriate Grignard reagent in benzene [5a]. The crude

Table 4

Rate constants, activation parameters and bond dissociation energies for $LFe(OEP)CH_3$ complexes in the presence of limiting concentration of added ligand

Ligand	k_1 (s^{-1} 25°C)	$\Delta H^{\ddagger}$ (kcal mol^{-1})	$\Delta S^{\ddagger}$ (cal (mol K)$^{-1}$)	D_{Fe-r} (kcal mol^{-1})
None	2.5×10^{-5}	23.3	−1.1	21
Pyridine	1.0×10^{4}	21.9	−3.2	20
PEt_3	1.7×10^{-2}	20.1	1.1	18

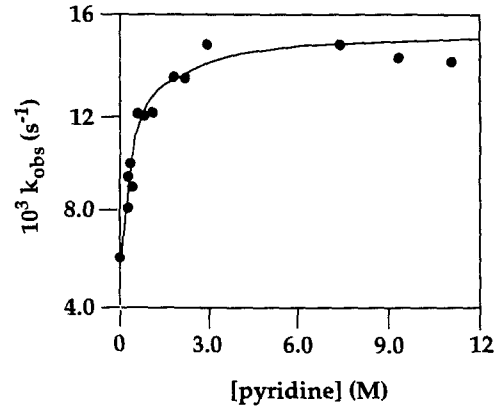

Fig. 5. Plot of k_{obs} versus [pyridine] for thermolysis of $Fe(OEP)CH_3$ (5.0×10^{-5} M) in the presence of Ph_3SnH (2.0×10^{-2} M) in benzene at 70°C. The best fit curve was calculated using the values, $k_{py} = 1.56 \times 10^{-2}$ s^{-1} and $K_D = 0.44$ M^{-1}.

products were purified by column chromatography on silated silica gel in a N_2-filled glove box. Compound purity was checked by ^1H NMR and UV-visible spectroscopy. Elemental analysis for $Fe(OEP)C_6H_5$: calc. for $C_{36}H_{44}N_4Fe$: C, 73.45; H 7.55. Found: C, 73.09; H, 7.48%. Fe(P) complexes were prepared by allowing solutions of the corresponding $Fe(P)CH_2C_6H_5$ to stand for several minutes at 30°C. The Fe–$CH_2C_6H_5$ bonds were rapidly homolyzed under these conditions yielding Fe(P) and toluene. Evaporation of the volatiles yielded pure Fe(P) as determined by ^1H NMR spectroscopy.

Proton NMR spectra were recorded on a QE 300 MHz spectrometer, Bruker Omega 500 or 300 MHz spectrometers. Spectra were referenced to residual protio solvent resonances. Deuterium and ^{119}Sn NMR spectra were recorded on the Bruker Omega 500 or 300 MHz instru-

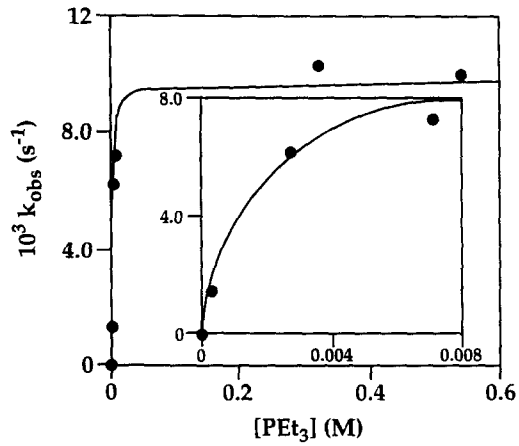

Fig. 6. Plot of k_{obs} versus [PEt_3] for thermolysis of $Fe(OEP)CH_3$ (5.0×10^{-5} M) in the presence of Ph_3SnH (2.0×10^{-2} M) in benzene at 20°C. The best fit curve was calculated using the values, $k_{PEt_3} = 9.7 \times 10^{-3}$ s^{-1} and $K_D = 1.6 \times 10^{-3}$ M^{-1}. Inset: expanded view of low [PEt_3] range.

ments. Deuterium spectra were referenced to natural abundance solvent resonances and ^{119}Sn spectra were referenced to Me_4Sn (0.00 ppm) as internal standard.

4.1. Kinetic measurements

Stock solutions of Fe(P)R ($R = CH_3$, C_6H_5) and Ph_3SnH were prepared in a N_2-filled glovebox. Due to their limited stabilities, fresh solutions of Fe(P)R ($R = C_2H_5$, $CH_2(CH_3)_3$ and $CH_2C_6H_5$) were prepared for each kinetic run. Aliquots were transferred to a 1 cm quartz spectrophotometric cell which was sealed under N_2 with a Kontes roto-seal tap. Kinetic measurements were made with a Perkin Elmer Lambda 7 spectrometer equipped with a thermostated cell block. Rates were measured by monitoring absorbance changes at 392 or 550 nm (545 nm for reactions with added axial ligand) corresponding to the disappearance of Fe(P)R. Selected experiments also were monitored at a wavelength (407 nm) corresponding to the appearance of Fe(P) to confirm that this rate agreed with the rate of disappearance of Fe(P)R. Values of k_{obs} were obtained from slopes of plots of $\ln|A - A|$ versus time over three half-lives. Duplicate runs typically agreed to within ±4%. Reactions with added base which were not in the saturation regime showed deviations from linearity after the first or second half-life. The deviations were consistently in the same direction, namely towards decreasing rates as the reactions progressed. For these experiments, rate constants were determined from the data for the first half-life only. In the limiting regime, all plots were linear through three half-lives.

Acknowledgements

This work was supported by the National Science Foundation and the National Institutes of Health.

References

[1] E.J. Corey, S.W. Wright and S.P.T. Matsuda, *J. Am. Chem. Soc., 111* (1989) 1452.

[2] (a) P.R. Ortiz de Montellano, O. Augusto, F. Viola and K.L. Kunze, *J. Biol. Chem., 258* (1983) 8623; (b) O. Augusto, K.L. Kunze and P.R. Ortiz de Montellano, *J. Biol. Chem., 257* (1982) 6231; (c) P.R. Ortiz de Montellano, K.L. Kunze and O. Augusto, *J. Am. Chem. Soc., 104* (1982) 3545; (d) D. Lancon, P. Cocolios, R. Guilard and K.M. Kadish, *J. Am. Chem. Soc., 106,* (1984) 4472.

[3] P. Battioni, J.P. Mahy, G. Gillet and D. Mansuy, *J. Am. Chem. Soc., 105* (1983) 1399.

[4] D. Dodd and M.D. Johnson, *J. Organomet. Chem., 52* (1973) 1.

[5] (a) P. Cocolios, G. LaGrange and R. Guilard, *J. Organomet. Chem., 253,* (1983) 65; (b) A.L. Balch and M.W. Renner, *Inorg. Chem., 25,* (1986) 303; (c) H. Ogoshi, H. Sugimoto, Z.I. Yoshida, H. Kobayashi, H. Sakai and Y. Maeda, *J. Organomet. Chem., 234* (1982) 185; (d) D.A. Clarke and A.W. Grigg Johonson, *Chem. Commun.,* (1966) 208; (e) D.A. Clarke, D. Dolphin and A.W. Grigg Johonson, *J. Chem. Soc. C,* (1968) 881.

[6] For O_2 insertion, (a) R.D. Arasasingham, A.L. Balch, C.R. Cornman and L. Latos-Grazynski, *J. Am. Chem. Soc., 111,* (1989) 4357; (b) A.L. Balch, R.L. Hart, L. Latos-Grazynski and T.G. Traylor, *J. Am. Chem. Soc., 112* (1990) 7382; (c) R.D. Arasasingham, A.L. Balch, R.L. Hart and L. Latos-Grazynski, *J. Am. Chem. Soc., 112* (1909) 7566. For CO and CO_2 insertion, I.M. Arafa, K. Shin and H.M. Goff, *J. Am. Chem. Soc., 110* (1988) 5228. For SO_2 insertion, P. Cocolios, E. Laviron and R. Guilard, *J. Organomet. Chem., 228* (1988) C39.

[7] M. Perree-Fauvet, A. Gaudemer, P. Boucly and J. Devynck, *J. Organomet. Chem., 120* (1976) 439.

[8] (a) Z. Li and H.M. Goff, *Inorg. Chem., 31* (1992) 1547; (b) B. Song and H.M. Goff, *Inorg. Chem., 33* (1994) 5979.

[9] T.-T. Tsou, M. Loots and J. Halpern, *J. Am. Chem. Soc., 104* (1982) 623.

[10] J. Halpern, *Polyhedron, 7* (1988) 1483, and references therein.

[11] D.J. Carlsson and K.U. Ingold, *J. Am. Chem. Soc., 90,* (1968) 7047.

[12] D. Brault and P. Neta, *J. Am. Chem. Soc., 103* (1981) 2705.

[13] (a) D. Lancon, P. Cocolios, R. Guilard and K.M. Kadish, *Organometallics, 3,* (1984) 1164; (b) K.M. Kadish, A. Tabard, W. Lee, Y.H. Liu, C. Ratti and R. Guilard, *Inorg. Chem., 30* (1991) 1542.

[14] (a) J.P. Collman, P.J. MeElwee-White, P.J. Brothers and E. Rose, *J. Am. Chem. Soc., 108* (1986) 1332; (b) M. Ke, S.J. Rettig, B.R. James and D. Dolphin, *J. Chem. Soc., Chem. Commun.,* (1987) 1110; (c) M. Ke, C. Sishta, B.R. James, D. Dolphin, J.W. Sparapany and J.A. Ibers, *Inorg. Chem., 30* (1991) 4766.

[15] (a) F.T.T. Ng, G. Rempel and J. Halpern, *Inorg. Chim. Acta, 77* (1983) L165; (b) M.K. Geno and J. Halpern, *J. Am. Chem. Soc., 109* (1987) 1238.

[16] M.K. Geno and J. Halpern, unpublished results.

[17] P. Doppelt, *Inorg. Chem., 23* (1984) 4009.

[18] D Lexa, J. Mispelter and J.M. Savéant, *J. Am. Chem. Soc., 103* (1981) 6806.